NEUROSCIENCE
RESEARCH ARTICLE

M. Sheroziya, R. Khazipov / Neuroscience 532 (2023) 50–64

Synaptic Origin of Early Sensory-evoked Oscillations in the Immature Thalamus

Maxim Sheroziya [a,*] **and Roustem Khazipov** [a,b]

[a] *Laboratory of Neurobiology, Kazan Federal University, Kazan, Russia*

[b] *Aix Marseille University, INSERM, INMED, Marseille, France*

Abstract—During the critical period of postnatal development, brain maturation is extremely sensitive to external stimuli. Newborn rodents already have functional somatosensory pathways and the thalamus, but the cortex is still forming. Immature thalamic synapses may produce large postsynaptic potentials in immature neurons, while non-synaptic membrane currents remain relatively weak and slow. The thalamocortical system generates spontaneous and evoked early gamma and spindle-burst oscillations in newborn rodents. How relatively strong synapses and weak intrinsic currents interact with each other and how they contribute to early thalamic activities remains largely unknown. Here, we performed local field potential (LFP), juxtacellular, and patch-clamp recordings in the somatosensory thalamus of urethane-anesthetized rat pups at postnatal days 6–7 with one whisker stimulation. We removed the overlying cortex and hippocampus to reach the thalamus with electrodes. Deflection of only one (the principal) whisker induced spikes in a particular thalamic cell. Whisker deflection evoked a group of large-amplitude excitatory events, likely originating from lemniscal synapses and multiple inhibitory postsynaptic events in thalamocortical cells. Large-amplitude excitatory events produced a group of spike bursts and could evoke a depolarization block. Juxtacellular recordings confirmed the partial inactivation of spikes. Inhibitory events prevented inactivation of action potentials and gamma-modulated neuronal firing. We conclude that the interplay of strong excitatory and inhibitory synapses and relatively weak intrinsic currents produces sensory-evoked early gamma oscillations in thalamocortical cells. We also propose that sensory-evoked large-amplitude excitatory events contribute to evoked spindle-bursts.**© 2023 IBRO. Published by Elsevier Ltd. All rights reserved.**

Key words: postnatal development, thalamic drivers, patch-clamp, early sensory-evoked oscillation, gamma events, urethane.

INTRODUCTION

Sensory-evoked and spontaneous neuronal activity plays an important role in network formation during development (Blankenship and Feller, 2010; Erzurumlu and Gaspar, 2012; Vitali and Jabaudon, 2014; Molnar et al., 2020). In line with this basic rule, somatosensory pathways in newborn rodents can transmit sensory signals to the immature cortex, which serves network maturation rather than sensation (Khazipov and Milh, 2018; Luhmann and Khazipov, 2018). During the first postnatal week in rodents, the cortex and thalamus generate short-term spontaneous and sensory-evoked gamma oscillations and early alpha/beta oscillations called spindle-bursts but remain silent most of the time at the LFP level (Minlebaev et al., 2007; Marcano-Reik and Blumberg, 2008; Yang et al., 2009; Minlebaev et al., 2011; Yang et al., 2013). It was proposed that the thalamus and periphery contribute to early gamma activity and spindle-bursts (Khazipov and Milh, 2018; Murata and Colonnese, 2019). The rodent cortex starts generating global adult-like patterns, i.e., persistent network activity during wakefulness and slow oscillations during sleep and general anesthesia, by approximately the end of the second week of postnatal development (Golshani et al., 2009; Murata and Colonnese, 2018; Dominguez et al., 2021).

The thalamus is the main gateway for sensory signals on their route to the cortex (Hwang et al., 2017). Thalamocortical cells of the relay thalamic nuclei receive sensory signals via large excitatory synapses (thalamic drivers) formed on proximal dendrites. Feedback corticothalamic axons form small synapses (thalamic modulators) on distal dendrites of thalamocortical cells in the relay nuclei. Thalamic higher-order nuclei receive drivers originating

*Corresponding author. Address: Karl Marks 76, Kazan, Tatarstan 420012, Russia.
E-mail address: mgsheroziya@gmail.com (M. Sheroziya).

Abbreviations: EPSPs, excitatory postsynaptic potentials; IPSPs, inhibitory postsynaptic potentials; LFP, local field potential; LTS, low-threshold spike; MUA, multiunit activity; PBS, phosphate-buffered saline; TRN, thalamic reticular nucleus; VPM, ventral posteromedial nucleus.

https://doi.org/10.1016/j.neuroscience.2023.09.005
0306-4522/© 2023 IBRO. Published by Elsevier Ltd. All rights reserved.

mainly from cortical layer V pyramidal neurons (Sherman and Guillery, 1996, 1998; Groh et al., 2014). Large amplitude and fast-rising excitatory postsynaptic potentials (EPSPs) recorded in thalamic cells *in vivo* are thought to be generated by thalamic drivers (Brecht and Sakmann, 2002; Deschenes et al., 2003; Ganmor et al., 2010; Sheroziya and Timofeev, 2014, 2015; Urbain et al., 2015; Mease et al., 2016). It has been shown on thalamic slices of newborn animals that NMDA receptors participate mightily in relay synapses (Ramoa and McCormick, 1994a; Arsenault and Zhang, 2006). Relatively weak ionic currents generated at immature synapses might produce large postsynaptic potentials in immature thalamic neurons (Ramoa and McCormick, 1994b). However, thalamic driver activity and its contribution to early oscillations have never been shown in newborn animals *in vivo*.

The low-threshold calcium T-current defines the intrinsic property of thalamic cells to produce low-threshold spike (LTS) bursts (Jahnsen and Llinas, 1984). Generation of LTS burst is mechanistically bound to a hyperpolarized membrane potential and fast transitions to a depolarized potential, which are features of slow-wave sleep and general anesthesia (Steriade et al., 1993; Crunelli et al., 2006; Llinas and Steriade, 2006; Timofeev and Chauvette, 2013; Fogerson and Huguenard, 2016; Fernandez and Luthi, 2020). In particular, thalamocortical and inhibitory cells in the thalamic reticular nucleus (TRN) generate rhythmic LTS bursts during thalamic sleep spindles. On the other hand, thalamic drivers produce either spike bursts or unitary spikes (bursting and tonic mode) in a membrane potential-dependent manner in thalamic relay cells (Castro-Alamancos, 2002). Behavioral state and behavior itself determine the thalamic firing mode in adult animals (Hirsch et al., 1983; Guido and Weyand, 1995; Ramcharan et al., 2000; Fanselow et al., 2001; Sherman, 2001; Marlinski and Beloozerova, 2014; Urbain et al., 2019). In thalamic slices of newborn animals, neurons generated weak LTS without spikes or with a burst of lower spike frequency. Immature cortical and thalamic neurons generated broad action potentials of smaller amplitude compared to mature activity (McCormick and Prince, 1987; Huguenard et al., 1988; Ramoa and McCormick, 1994b; Perez Velazquez and Carlen, 1996; Pirchio et al., 1997; Tennigkeit et al., 1998; Luhmann et al., 2000; Lee et al., 2010). Despite of weakness of voltage-gated intrinsic currents, the resting membrane potential estimated with advanced methods in immature neurons is as hyperpolarized as in mature neurons (Tyzio et al., 2003; Yakovlev et al., 2013). The polarized resting membrane potential is probably a common property of all cell types (Abdul Kadir et al., 2018). Weak intrathalamic inhibitory feedback from TRN is already present in newborn rodents (Warren and Jones, 1997; Evrard and Ropert, 2009; Lee et al., 2010). In ferret slices of the lateral geniculate nucleus, spindle oscillations appeared at 3–4 weeks of age (McCormick et al., 1995).

Because of methodological difficulties, cellular mechanisms underlying early activities remain largely unknown or contradictory. Therefore, we tested sensory-evoked intracellular and juxtacellular thalamic activities in the thalamus of urethane-anesthetized rat pups at postnatal days 6 and 7 (P6-7). Corticothalamic connections were inactive because we removed the overlying somatosensory cortex. Sensory-evoked rhythmic large-amplitude EPSPs (likely thalamic drivers) produced spike bursts/plateau potentials in thalamocortical cells. Membrane potential depolarization with current injection did not prevent bursting activity. Gamma-modulated inhibitory postsynaptic potentials (IPSPs) likely originating from TRN transformed spike bursts/plateau potentials into short gamma events.

EXPERIMENTAL PROCEDURES

Ethical approval

Experiments were performed in accordance with EU Directive 2010/63/EU for animal experiments, and the animal-use protocols were in line with Kazan Federal University on the use of laboratory animals (ethical approval by the Institutional Animal Care and Use Committee of Kazan State Medical University N9-2013).

Surgery

Animals were housed at the animal facility with controlled temperature, natural light cycle, ventilation, and low noise level. After birth, rat pups were housed with their maters in standard cages. 34 rat pups (6–7 days old, P6-7; sex was not taken into consideration) were used in this study. During surgery, we used inhalation anesthetic isoflurane (concentration 2–4%; EZ-7000 classic system, E-Z Systems). We started with 4% isoflurane and decreased concentration by the end of surgery (with inspection of the surgical plane of anesthesia and constant visual inspection of breathing). We injected urethane (1–1.3 g/kg, intraperitoneal injection) by the end of surgery; used dosage of urethane provided general anesthesia during the experiments, which lasted 4–6 h. Then we placed the anesthetized animals in a short tube on a warm thermal pad (37 °C) and carefully covered them with cotton wool. Animals were placed in a sitting fetal position in the tube, and the head was bent forward relative to the body. The sitting fetal position allowed the fourth ventricle to be opened (see below) in rat pups that have short necks. Surgical instruments and surfaces were cleaned with soap water and alcohol. The skull of the animal was cleaned of skin with scissors and a scalpel and cleaned of tissues with 0.3% peroxide. The head was fixed in the stereotaxic frame with metal plates, dental cement, and cyanoacrylate glue. We drilled a large cranial window above the left hemisphere (from bregma to lambda and from 0.2–0.3 mm to 5–6 mm lateral from a midline). Using the cranial window whole accessible cortex and the hippocampus (partly) were gently removed with suction. To remove brain tissues, we used small single-used plastic pipettes. To reduce pulsations, the obtained recess was covered with paraffin (1/3 part) in mineral oil during all thalamic recordings. We covered the recess

when electrodes touched the thalamic surface. To reduce brain pressure and pulsation, we also opened the fourth ventricle after drilling. We used a chlorinated silver wire placed on the cerebellum for a reference electrode. In the experiments with silicon probes, to show that the upper part of the hemisphere did not contribute to the thalamic response, we removed the whole upper part of the left hemisphere (Fig. 1; lateral: from 0.2–0.3 mm to 4–6 mm from a midline; anteroposterior: from −3 mm to lambda).

Extracellular and patch-clamp thalamic recordings

All recordings were obtained in the left hemisphere under general anesthesia. Thalamic local field potential (LFP) recordings were obtained with linear silicon probes (50 μm spacing between the recording sites, NeuroNexus Technologies, USA). To visualize traces, the probes were covered with fluorescent (green light) dye (1,1′-dioctadecyl-3,3,3′,3′-tetramethylindocarbocyanine perchlorate, Sigma). LFP signals from the probes were acquired using a Digital Lynx amplifier (Neuralynx, USA), digitized at 32 kHz, and saved for post hoc analysis. We used tungsten needle microelectrodes for juxtacellular recordings (tip resistance 4–5 MΩ, Microelectrodes, Cambridge, UK). Using a micromanipulator (Sutter Instrument, USA), we slowly immersed electrodes into the thalamus to a depth of ∼1–1.5 mm (Khazipov et al., 2015) and located vibrissae-evoked responses. Similarly to the adult thalamus, a particular thalamic cell responded with spikes to deflection of only one whisker (the principal whisker). We detected a principal whisker manually in each experiment, and then a plastic tube (1 mm tip diameter) connected to Pneumatic PicoPump (WPI, USA) was fixed ∼1 mm from the whisker for air-puff stimulation. Similarly

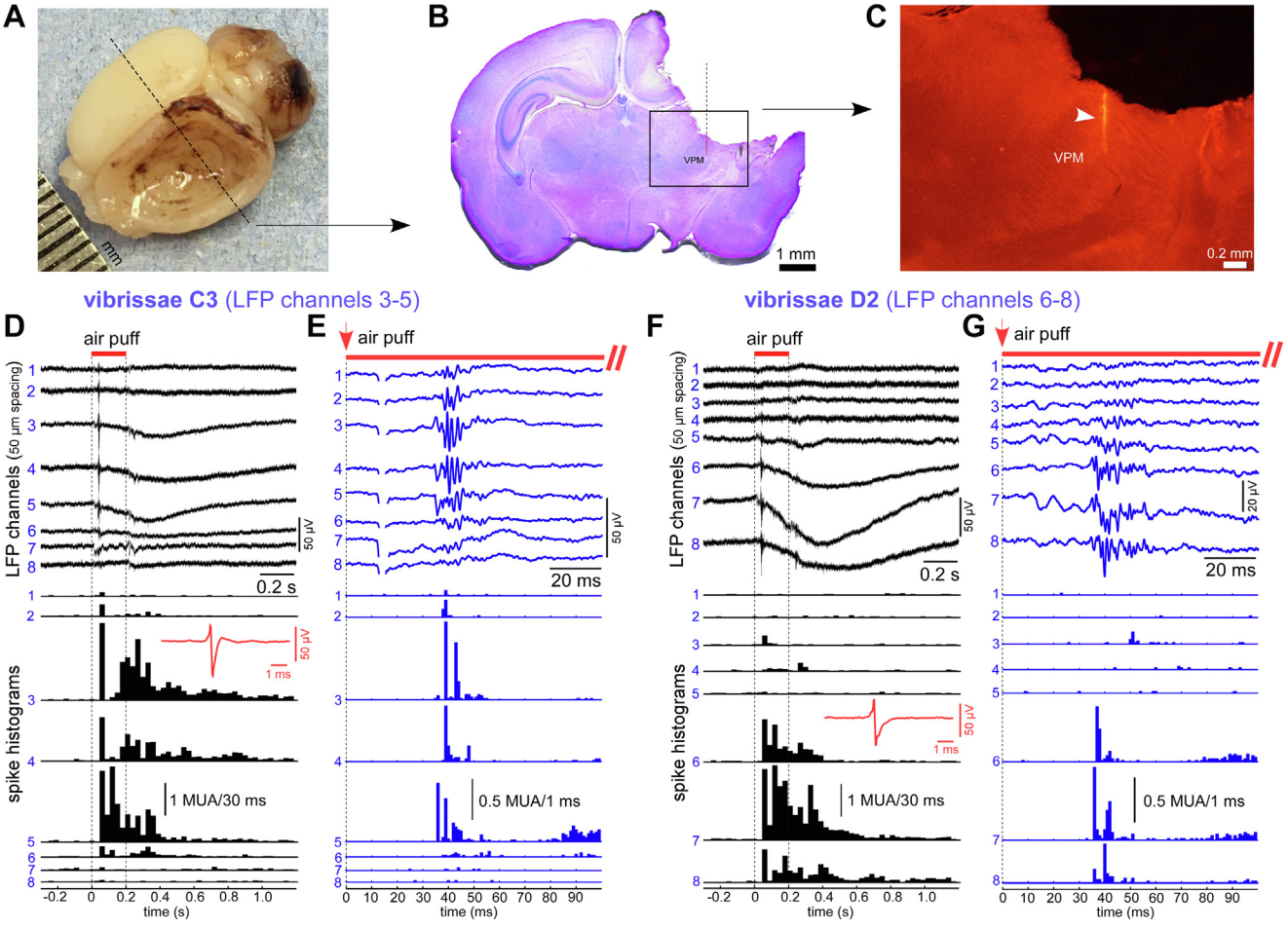

Fig. 1. Sensory-evoked thalamic responses obtained with a linear silicon probe (low-impedance LFP electrodes). (**A**) A photo of a formalin-fixed rat brain. The majority of the upper cortex and hippocampus were removed. The dashed line schematically indicates the location of the frontal section shown in B. (**B**) Light photograph shows the frontal section stained with cresyl violet. (**C**) Fluorescent trace of the silicon probe in the thalamus. Before staining with cresyl violet, the trace of the silicon probe was detected in green light. (**D**) Average (60 trails, vibrissae C3) whisker-evoked LFP response with peristimulus time histograms (below) recorded in the brain shown in A, B, and C with a linear silicon probe (8 of 16 channels shown, 50 μm spacing between recording sites). Channel numbers are shown in blue. The red line represents the air puff (duration 0.2 s). Peristimulus time histograms represent MUA spiking of the corresponding LFP channels (see channel numbers). An example of an average MUA spike is shown in red. (**E**) The onset of the sensory-evoked response shown in D. The red arrow represents air puff onset. (**F**) Average (60 trails) LFP response with peristimulus time histograms (below) evoked with an air puff stimulation of a neighboring vibrissae D2. An example of an average MUA spike is shown in red. Note that the sensory-evoked response was longer than the stimulus duration. (**G**) The onset of the sensory-evoked response shown in F. Red arrow represents air puff onset.

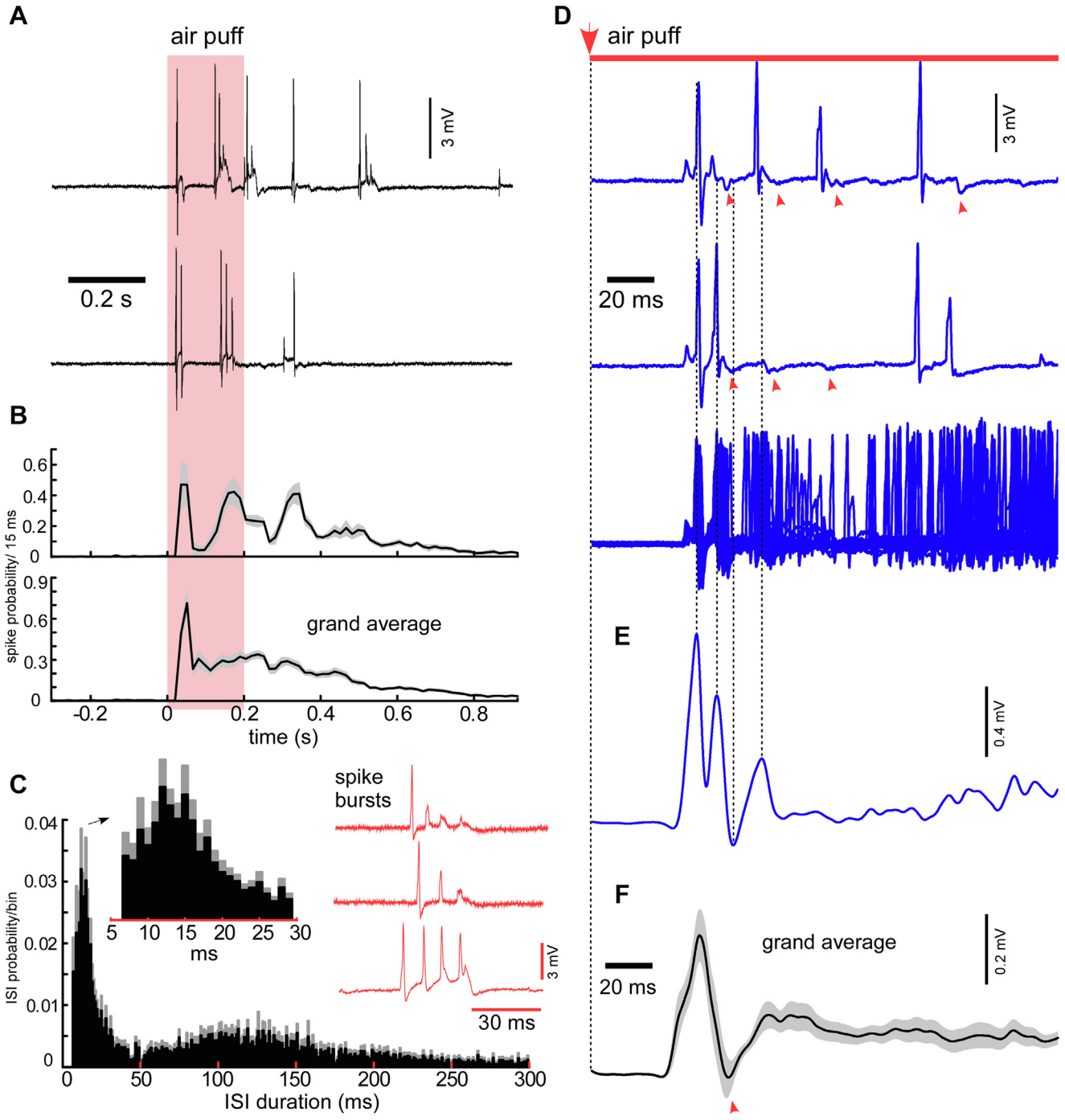

Fig. 2. Juxtacellular thalamic responses recorded with a high-impedance extracellular electrode. (**A**) Two examples of sensory-evoked responses. One-whisker stimulation elicited a series of spike bursts in thalamic cells. Air-puff stimulation is shown in pink. (**B**) Average peristimulus time histograms represent a thalamic spiking response. A majority of thalamic cells displayed a tendency to fire in bursts every 100–200 ms after sensory stimulation. The upper histogram shows the average response for 9 recordings (60 trails for each recording) which displayed similar inter-burst intervals. The bottom histogram shows the grand average sensory-evoked response (n = 31 recordings, 60 trails for each recording). (**C**) Bimodal distribution of inter-spike intervals (ISIs) during sensory-evoked response. In 14 (~45%) juxtacellular recordings, ISI distribution displayed 2 peaks corresponding to intra-burst and inter-burst intervals. An example of a spike burst is shown in red. (**D**) Two examples of the onset of the sensory-evoked spiking response and a superposition of 60 trails (below). Note negative peaks, which are indicated with red arrows. (**E**) Spiking responses shown in D form oscillation after averaging (60 trails). The responses were smoothed with a low-pass filter (100 Hz) and averaged. (**F**) Grand average thalamic spiking response (n = 31 recordings, 60 trails for each recording).

to the tungsten electrodes, patch pipettes were slowly inserted with a micromanipulator (Sutter Instrument, USA) to the same depth. In rat pups, most thalamic neurons maintained low concentration of intracellular chloride and were inhibited by GABA (Glykys et al., 2009). Therefore, we used intracellular solutions with low concentra-

tions of intracellular chloride corresponding to the inhibitory action of GABA. For current-clamp recordings patch pipettes were backfilled with the following (in mM): 144 K-gluconate, 4 KCl, 10 disodium phosphocreatine, 10 HEPES, 4 MgATP, and 0.3 GTP, pH 7.3 (tip resistance ~7 MΩ); for voltage-clamp (in mM): 144 Cs-gluconate, 4 CsCl, 10 disodium phosphocreatine, 10 HEPES, 4 MgATP, and 0.3 GTP, pH 7.3 (tip resistance ~7 MΩ) with or without 5 mM QX-314 (bromide). Series resistance was 30–60 MΩ. To visualize thalamic cells, the pipettes were filled with 0.5% biocytin (Sigma). Juxtacellular and intracellular signals were acquired with a MultiClamp 700B amplifier (Molecular Devices, USA), digitized at 32 kHz, and saved for post hoc analysis.

We positioned the air puff tube to deflect one whisker on the right side of the snout under visual control. Sensory stimulation was performed with 200-ms-long air puffs every 10 s. To obtain stable and stereotyped sensory-evoked thalamic responses, we used an air puff intensity 2–3 times higher than the minimal intensity, which was able to produce a response (air pressure adjusted with the Pneumatic PicoPump; 5–10 Psi; Fig. S2). Used air puffs led to ~1 mm whisker deflection and could produce high-frequency vibration (~300 Hz, detected with a high-speed camera, not shown), but we did not detect vibrations within the gamma frequency range. Using a piezoelectric sensor, we measured the delay (~12.5 ms) between the actuation of the Pneumatic PicoPump and the onset of the air puff at the other end of the tube (Fig. S1). To calculate response latencies, we took into account the 12.5 ms delay between the recorded actuation times of the Pneumatic PicoPump and the whisker's deflection with the air puff.

Histochemistry

After recordings, deeply anesthetized animals were perfused with 0.1 M phosphate-buffered saline (PBS) followed by 4% PFA in PBS. Then, the brains were removed and stored overnight in 4% PFA in PBS at 4 °C. Then 70-μm-thick frontal sections were obtained with a vibratome (Microm HM 650 V, Thermo Scientific), extensively rinsed, and incubated in 0.3% H_2O_2 in PBS for 2 h. To visualize biocytin-labeled cells, free-floating sections were incubated in an ABC kit (1:200; Vector Laboratories), 0.1% Triton X-100 (Panreac), and 1% bovine serum albumin in PBS for 3 h. After rinsing, sections were incubated in PBS containing 0.05% DAB (Sigma) and 0.00125% H_2O_2 for 5–10 min.

Data analysis and statistics

Signals were analyzed using built-in functions and custom-developed MATLAB scripts (MathWorks, USA). To detect multiunit activity (MUA) in LFP recordings (silicon probes), we high-passed (100–15,999 Hz) the raw wide-band signal, differentiated the signal, calculated standard deviation (SD), and then located negative peaks below a threshold of 4–5 SD. The detected MUA were averaged and visually inspected. For spike detection in juxtacellular recordings, we used a threshold of 2–4 mV for the raw signals (with a visual inspection). For each extracellular recording, we plotted a peristimulus time histogram and detected latency (the first bin with a value above zero) for sensory-evoked spikes. For spectrograms (Figs. 3, 4, and S5(**E**)), we re-sampled the raw signals from 32 kHz to 1 kHz, set the baseline to zero, calculated a spectrogram for each sensory-evoked response (Hamming window 328 ms), and averaged the spectrograms. To produce a similar and comparable spectral analysis for MUA activity obtained with silicon probes (Fig. S3), we used a high-pass filter (> 1.5 kHz) and smoothed LFP signals; then, we calculated the spectrograms as described above. To compare spectrums of intracellular sensory-evoked currents (Fig. 4(**C**)), we re-sampled the raw signals from 32 kHz to 1 kHz, set the baseline to zero, normalized each response on its mean absolute deviation, and then calculated the spectrum. To detect significant differences, we employed the nonparametric Wilcoxon signed rank test. To detect IPSCs (Fig. 4(**H**)), we differentiated the signals, calculated SD, and located positive peaks above 2 SD. For EPSCs, we differentiated the raw signals and located negative peaks below 32 pA/ms. In the figures, the data are expressed as mean value ± SEM. In the text, the data are expressed as mean value ± SD.

RESULTS

LFP and juxtacellular thalamic responses to one-whisker stimulation in rat pups

We recorded vibrissae-evoked responses in the thalamic ventral posteromedial nucleus (VPM) using linear silicon probes with 50 μm spacing between the recording sites. The silicon probes were covered with a fluorescent dye to locate traces after recordings. We removed all accessible upper cortex and hippocampus before recordings so that the barrel cortex could not provide feedback to the thalamus. In the experiments with silicon probes, to show that the upper part of the hemisphere did not contribute to the thalamic response, we removed the whole upper part of the left hemisphere (Fig. 1). Average LFP response (60 trails averaged) composed of a short-term ripple or gamma oscillation followed by a long (up to 1 s) slow negative shift was detectable in 3–4 LFP channels. The amplitude of the slow negative shift varied from 30 μV to 180 μV in our recordings (n = 3 rats). In the shown example (Fig. 1), we successively recorded LFP responses from two neighboring whiskers in a given location. Sensory stimulation of the first vibrissae (C3) produced a response in channels 3–5, while the second vibrissae (D2) evoked a response in channels 6–8 (the channels at the tip of the silicon probe). Stimulation of other whiskers did not evoke a response in the shown location of the silicon probe. We detected MUA for each LFP channel and plotted average peristimulus time histograms revealing a similar depth profile to sensory responses (Fig. 1). In two other recordings with silicon probes (not shown), MUA responses covered four channels of the silicone probe with 50 μm spacing between the recording sites. Thus, the detected vertical

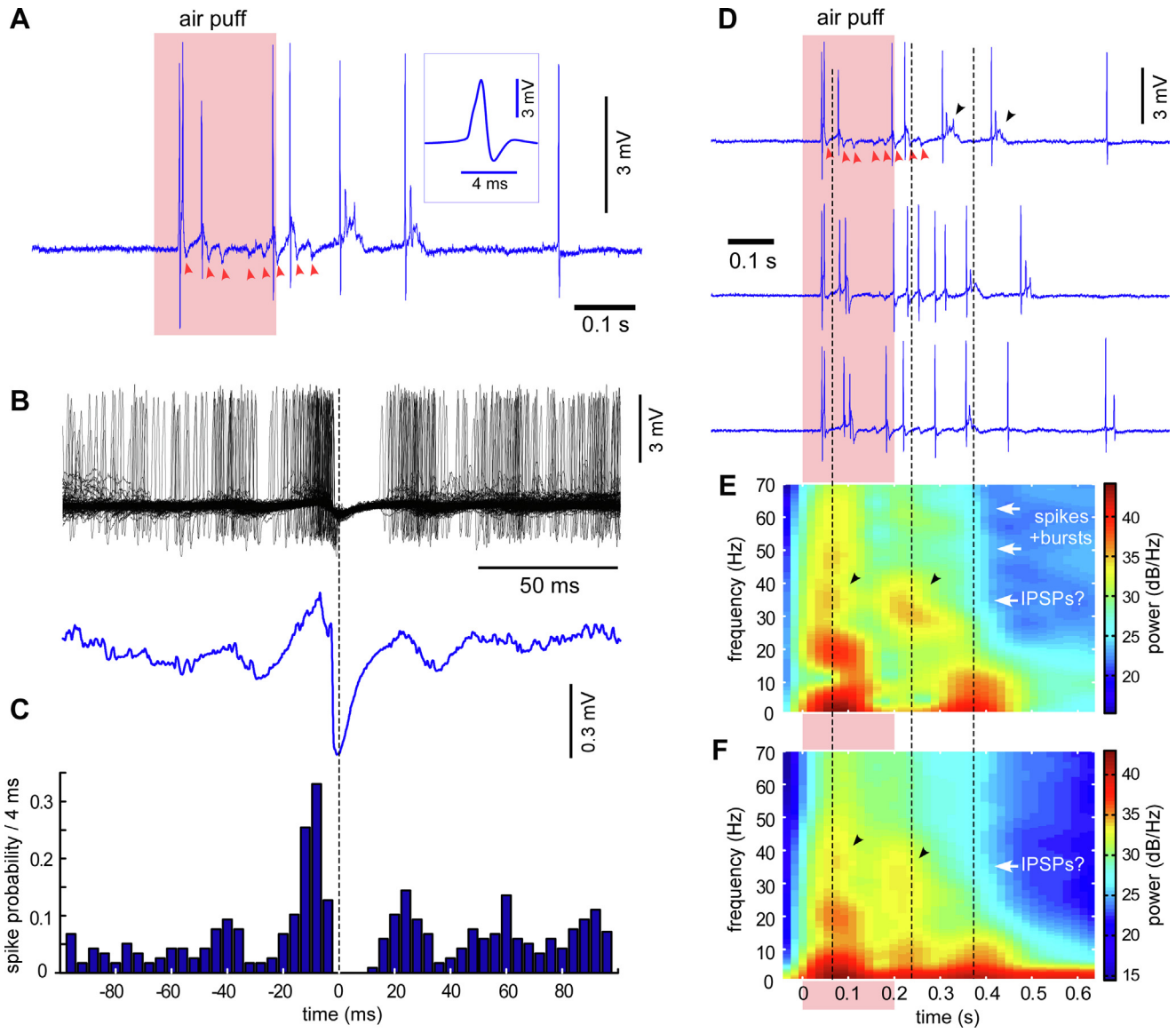

Fig. 3. Sensory-evoked gamma oscillations in the thalamus of rat pups. (**A**) Gamma-modulated thalamic spiking activity during sensory-evoked response. An example of the average spike is shown in a frame. Small-amplitude negative peaks are shown with red arrows. (**B**) An auto-correlogram triggered with the negative peaks. The superposition of spikes is shown in black. The average auto-correlogram is shown in blue. (**C**) A histogram represents spikes shown in B. (**D**) Three examples of sensory responses modulated in the gamma frequency range. In the first example, the negative peaks are shown with red arrows. Likely the same thalamic cell could generate spike bursts (shown with black arrows). (**E**) The average spectrogram was calculated for 60 trails for the juxtacellular recording shown in D. ''Hot spots" within the gamma frequency range marked with black arrows. (**F**) Average spectrogram for 7 recordings (60 trails for each recording), which displayed similar negative peaks (see D) and gamma hot spots (marked with black arrows).

size of thalamic barreloids was 150–200 μm. On average, 1–2 silicon probe channels with stronger response displayed shorter response latency, and 1–2 boundary channels showed longer latency: with a minimal latency of 23 ± 1 ms and a maximal 28 ± 1 ms. The duration of the response varied from 1 to 5 s. In the present study, we used 200-ms-long air puffs for one-whisker stimulation. Strictly speaking, airflow could deflect neighboring whiskers that were in line with the air puff tube. Since we could detect the bounds of thalamic barreloids, the air puff stimulation was local enough for our purposes.

In all experiments, we used an air puff intensity 2–3 times higher than the minimal intensity that produced a thalamic response. LFP and juxtacellular thalamic responses evoked with weaker and stronger air-puff stimulation are shown in Fig. S2. Stronger stimuli evoked pronounced poststimulus thalamic activity in the example shown with juxtacellular recording (Fig. S2(**C**)). Air-puff stimulation did not elicit long-lasting whisker deflection, which we checked with a high-speed camera (not shown).

To investigate the sensory-evoked spiking activity, we recorded thalamic responses with juxtacellular electrodes (n = 31 recordings in 16 pups). Needle tungsten electrodes (tip size ~10 μm) allowed us to record extracellular ~5 mV amplitude spikes from 1 to 2 thalamic cells (large-amplitude spikes probably were

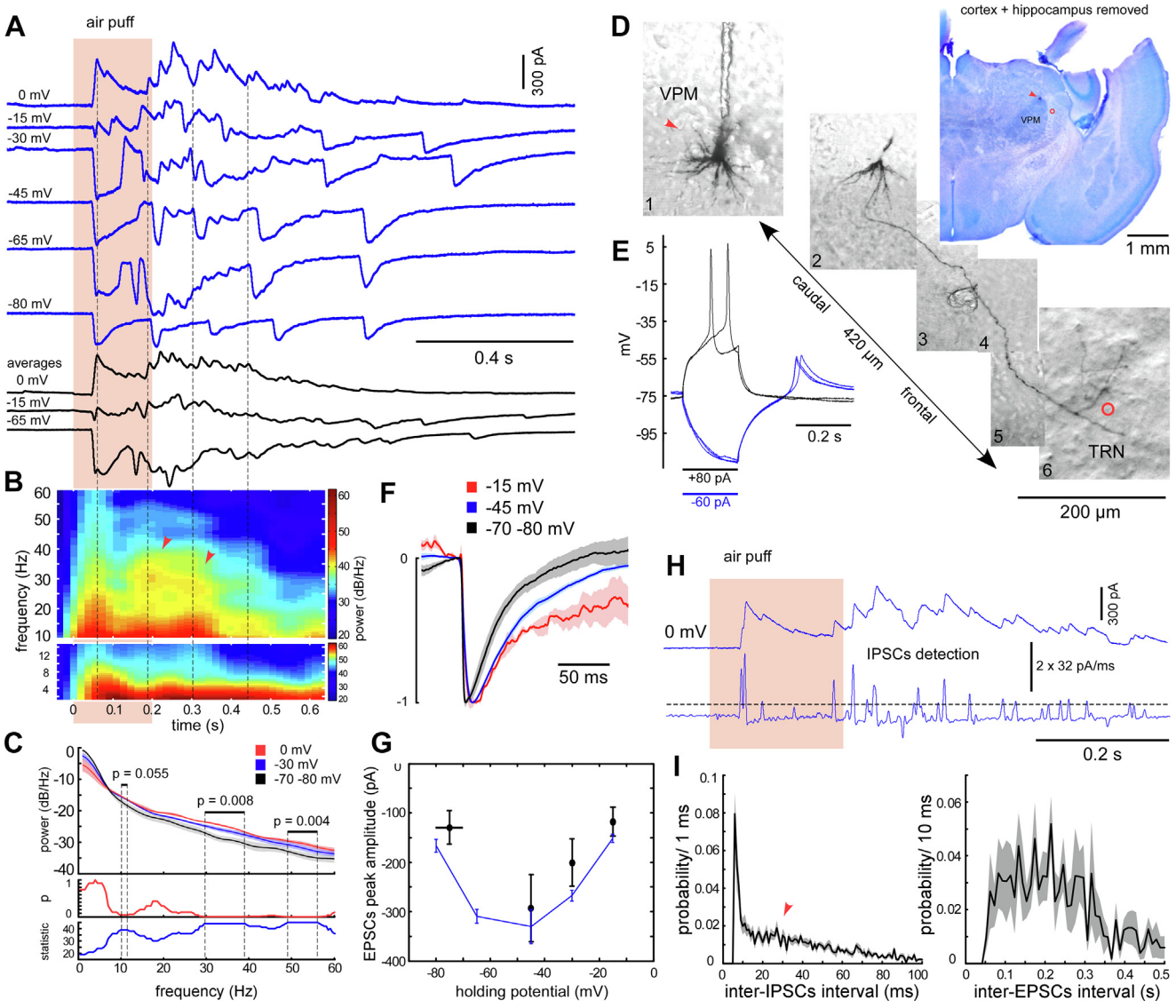

Fig. 4. Voltage-clamp recordings from thalamic cells revealed sensory-evoked excitatory and inhibitory postsynaptic currents. (**A**) Sensory-evoked intracellular currents recorded at different membrane potentials in the biocytin-stained thalamocortical cell shown in D. Average responses are shown below in black (6–10 trails averaged). The pink area represents air-puff stimulation. The recording was performed with a Cs-gluconate-based pipette solution with QX-314. (**B**) Average spectrogram calculated for 10 responses recorded at 0 and −15 mV holding membrane potential, one of which is shown in A. Hot spots within the gamma frequency range are marked with red arrows. Note the approximate coincidence of gamma hot spots with large EPSCs (vertical dashed lines). (**C**) Comparison of the response spectrums at different holding membrane potentials. Each response was normalized on its mean absolute deviation before spectrum calculation (see methods). The upper plots represent averaged spectrums for 3 holding membrane potentials (0, −30, and −70–80 mV; n = 9 cells). The bottom plots display the p-value and value of the Wilcoxon signed rank test statistic (0 mV vs. −70–80 mV). The gamma power of the sensory-evoked responses was significantly higher at 0 mV compared to the hyperpolarized membrane potential. (**D**) Biocytin-stained thalamocortical cell with a reconstructed axon. Cresyl violet-stained frontal section is shown in the upper right corner (the biocytin-stained cell is marked with a red arrow). Combined 6 grayscale images represent the stained cell with its axon, which gives collateral in TRN (marked with a red circle). (**E**) Cellular responses to depolarizing and hyperpolarizing current pulses obtained in current-clamp mode immediately after cell opening. Note LTS without spikes (blue). (**F**) The shape of sensory-evoked EPSCs depended on the holding membrane potential (grand average, n = 7). (**G**) The peak amplitude of sensory-evoked EPSCs depended on the holding membrane potential (black, n = 7 cells). EPSC peak amplitudes for the example recording in A are shown in blue. (**H**) Detection of sensory-evoked IPSCs. Examples of intracellular signal at 0 mV holding membrane potential and differentiated signal with a threshold (dashed line). We detected inter-IPSCs intervals > 5 ms. (**I**) Average distribution of inter-IPSCs (left, n = 9 cells) and inter-EPSCs (right, n = 7 cells) intervals during sensory-evoked responses. Liquid junction potential correction (15 mV subtraction) was applied to all scales.

generated by one cell). In all experiments, thalamic cells responded with spikes to deflection of only one (the principal) whisker. Sensory stimulation evoked a series of spikes and spike bursts, which tended to form 100–200 ms intervals (Fig. 2). We detected spikes and plotted time peristimulus histograms. The latency of the spike response was 29.9 ± 4.2 ms. Average stereotypic responses formed an oscillation-like pattern within the alpha frequency range (Fig. 2(**B**)). We calculated the distributions of inter-spike intervals (ISIs)

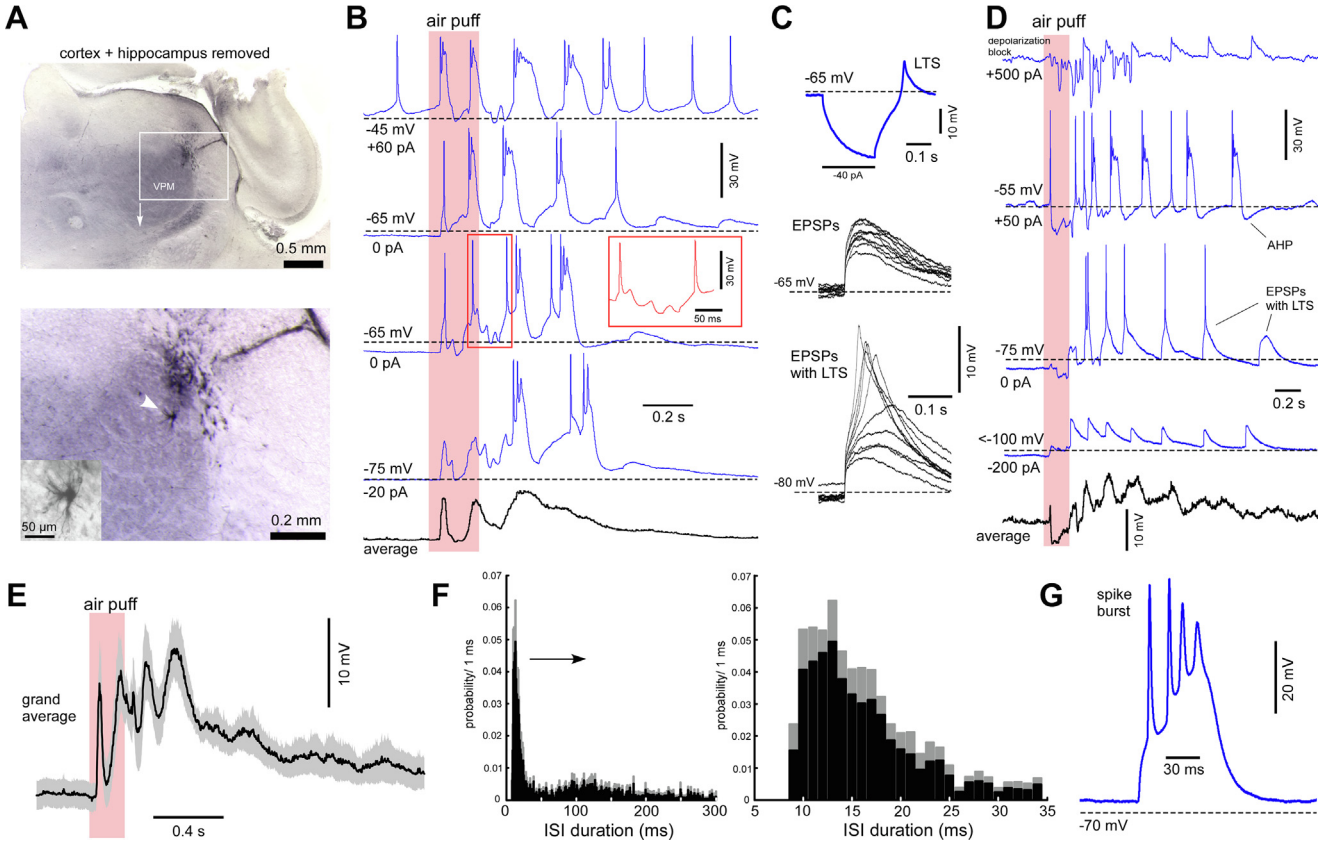

Fig. 5. Sensory-evoked large-amplitude EPSPs produce spike bursts modulated with IPSPs. (**A**) Frontal section with a thalamocortical cell stained with biocytin during patch clamp recording. Positive pressure in the patch pipette on its way to VPM led to extracellular staining with spilled biocytin. The cell was approached without pressure in a pipette, which explains the gap between the cell (marked with an arrow) and the dark area. (**B**) Examples of sensory-evoked responses of the cell shown in A. To change membrane potential, we applied constant current injections (indicated next to the examples). Note modulation by IPSPs shown in the red frame. An average response (60 trails) is shown below in black. (**C**) Thalamic cells generated rebound LTS after a negative current pulse without spikes (blue, same cell as in A and B). Large-amplitude EPSPs could generate LTS in a membrane potential-dependent manner (superposition of selected EPSPs (−65 mV) and EPSPs with LTS at the hyperpolarized membrane potential (−80 mV), black, same cell as in A and B). (**D**) Another example of current-clamp recording from a thalamocortical cell. Depending on the membrane potential sensory-evoked EPSPs produced LTS with single spikes (-75 mV) and spike bursts/plateau potentials (−55 mV), probably enhanced with NMDA currents. Note the afterhyperpolarization potential (AHP). Mixed excitatory and inhibitory postsynaptic activity at the beginning of the response did not generate rhythmic bursts. (**E**) Average sensory-evoked response recorded in current-clamp mode (grand average, $n = 7$ cells). (**F**) ISI distribution of intracellular activities displayed 2 peaks corresponding to intra- and inter-burst intervals ($n = 7$ cells). (**G**) An example of a sensory-evoked spike burst. Liquid junction potential correction (15 mV subtraction) was applied to all scales.

to quantify bursting activity. 45% of juxtacellular recordings ($n = 14$) displayed bimodal distribution with distinct peaks corresponding to intra-burst and inter-burst intervals (Fig. 2(**C**)). Peak locations corresponding to intra-burst and inter-burst intervals were 13.5 ± 2.3 m s and 118 ± 34 ms (range 83–205 ms), respectively. ISI distributions calculated for other recordings did not show two peaks because we could detect only the first spikes in bursts (spike amplitude decreased in bursts). Compared to the adult thalamus, intra-burst spike frequency in pups was smaller. The bursts did not show an ISI increase with ISI ordinal in a given burst (examples in Fig. 2(**C**)), a known feature of LTS bursts in thalamic cells (Lenz et al., 1994; Jeanmonod et al., 1996; Wei et al., 2011). Instead, strong excitatory postsynaptic events could produce sensory-evoked spike bursts (see below). We observed spontaneous transitions between tonic and bursting firing in one juxtacellular recording (the only recording with spontaneous bursting). These bursts displayed ISI increase with ISI ordinal in a given burst (Fig. S3; comparison of spontaneous LTS and sensory-evoked activity).

Stereotypic neuronal spiking at the beginning of the responses led to oscillation-like patterns after averaging (Fig. 2(**E**)). In seven recordings, we distinguished low-amplitude negative peaks (marked with red arrows in Fig. 3). Since the negative peaks were in opposition to spikes (Fig. 3(**A**), 3(**B**), and 3(**C**)), they could represent intracellular hyperpolarizing and inhibitory events (see below). Rhythmic low-amplitude negative peaks produced oscillatory patterns within the gamma frequency range during sensory response. To reveal oscillations, we re-sampled raw signals to 1 kHz, calculated a spectrogram for each trail, and then plotted an average spectrogram (Fig. 3(**E**)). Low-amplitude negative peaks resulted in 'hot spots' within the gamma frequency range in spectrograms (marked with black arrows in Fig. 3(**E**) and 3(**F**)). To reveal gamma-

modulated MUA, we transformed MUA spikes into a wave (high-passed > 1.5 kHz and smoothed raw signal) and calculated spectrograms (Fig. S4). MUA recorded with a silicon probe produced hot spots within the gamma and beta frequency ranges in spectrograms (Fig. S4(**C**)).

Based on the obtained extracellular data, we proposed that sensory stimulation evoked a series of relatively strong excitatory postsynaptic events able to produce spike bursts which, in turn, are gamma-modulated with inhibitory events.

Patch-clamp recordings of sensory-evoked responses in the thalamus of rat pups

We used a patch-clamp technique to verify that thalamic responses were composed of excitatory postsynaptic events and modulated with inhibitory events. As above, we removed the cortex and hippocampus. Immediately after the break-in, we applied the current steps in current-clamp mode. Thalamic cells generated LTS without spikes after a hyperpolarizing current step (Fig. 4(**E**)). We performed voltage-clamp recordings with Cs-gluconate-based solution with and without QX-314 (n = 9 cells in seven pups). We could clamp a membrane potential in a range from ∼0 mV to ∼−70 mV (Fig. 4(**A**)), though, in the experiments without QX-314, spikes sporadically occurred at hyperpolarized potentials (not shown). Cell input resistance was 0.46 ± 0.07 GΩ. The thalamic sensory-evoked response consisted of a series of excitatory postsynaptic currents (EPSCs) and inhibitory postsynaptic currents (IPSCs). EPSCs were distinguished at hyperpolarized potentials, and IPSCs manifested at depolarized membrane potentials (Fig. 4 (**A**)). The mean number of EPSCs per response was 5.13 ± 1.8 (range 3–9). In the example of a biocytin-stained thalamocortical cell shown in Fig. 4(**D**), the reconstructed axon of the cell gives collateral in TRN. The latter indirectly confirms that TRN provided inhibitory feedback to VPM during sensory-evoked responses in rat pups.

A spectrogram calculated for sensory-evoked responses at depolarized membrane potentials revealed hot spots within the gamma frequency range (Fig. 4(**B**)), comparable to the gamma activity observed in the juxtacellular recordings. Accordingly, the gamma power of sensory-evoked currents significantly decreased at a membrane potential of −70 mV compared to 0 mV (n = 9 cells; Fig. 4(**C**)). We also detected sensory-evoked EPSCs and checked their dependency on the holding membrane potential (Fig. 4(**F**) and 4(**G**)). In agreement with previously reported data (Ramoa and McCormick, 1994a; Arsenault and Zhang, 2006), the non-linear voltage-current dependency of peak amplitudes and the different shapes of EPSCs indicated that strong NMDA receptor-mediated current contributed to sensory-evoked EPSCs in VPM of rat pups. We detected postsynaptic events, calculated inter-IPSCs, and inter-EPSCs intervals, and plotted their distributions. In contrast to many electrophysiological distributions, which have an exponential right tail (Buzsaki and Mizuseki, 2014), inter-IPSC distribution displayed a plateau around 20–40 ms intervals (Fig. 4(**I**)). The peak location for inter-EPSC interval distribution was 183.6 ± 84.6 ms (range 90 – 300 ms). Both distributions show that corresponding sensory-evoked postsynaptic events tended to generate rhythms.

To observe intracellular spiking activity, we performed current-clamp recordings with a K-gluconate-based pipette solution (n = 7 cells in seven pups, Fig. 5). After a hyperpolarizing current step, thalamic cells generated LTS either without spikes or with one spike, and the input resistance was 0.44 ± 0.09 GΩ. Whisker deflection evoked a series of spike bursts/plateau potentials modulated with inhibitory potentials. To compare sensory-evoked responses at different membrane potentials, we applied constant current. Large-amplitude excitatory postsynaptic potentials (EPSPs) produced LTS in a membrane potential-dependent manner (Fig. 5(**B**) and 5(**D**)). Similarly to extracellular recordings, the ISI distribution of intracellular sensory-evoked activities displayed two peaks corresponding to intra- and inter-bursts intervals (Fig. 5(**F**)). Peak locations of intra-burst and inter-burst ISI distributions were 12.7 ± 1.8 ms and 108 ± 12 ms, respectively. The intra-burst peak was more pronounced for intracellular recordings (peak amplitude ∼0.5 probability/1 ms) compared to the intra-burst peak for juxtacellular recordings (peak amplitude ∼0.3 probability/1 ms, Fig. 5(**C**)) because spike amplitudes in a given extracellular burst decreased with the number of the spike in the burst and were not detected with a constant threshold (see Experimental Procedures).

To confirm our findings, we performed thalamic recordings with an intact cortex. We observed similar sensory-evoked activities with juxtacellular electrodes: sensory stimulation produced a series of spike bursts in the thalamus (not shown). We used K-acetate-filled sharp electrodes to record intracellular thalamic activities with an intact cortex. Compared to patch pipettes, the sharp electrodes produced shunting effects in immature thalamic cells. The cell input resistance was about 0.1 GΩ (vs. ∼0.45 GΩ with patch recordings), and large-amplitude EPSPs produced unitary broad spikes (not shown). We also performed LFP recordings in the barrel cortex (depth 0.4 mm) and calculated spectrograms for sensory-evoked activities (Fig. S5). We observed hot spots in the gamma frequency range similar to those we plotted for thalamic recordings. We conclude that the somatosensory thalamus might entrain the cortical cells in graded gamma oscillations.

DISCUSSION

We explored intracellular sensory-evoked activities from the thalamic VPM nucleus in rat pups. Since the whole-cell patch-clamp technique changes the intrinsic properties of small neurons with high input resistance (Tyzio et al., 2003), we also used extra- and juxtacellular electrodes and compared obtained results. Deflection of only one whisker induced spikes in a given thalamic cell. Sensory stimulation evoked a series of large-amplitude excitatory events, which produced weak LTS in a mem-

brane potential-dependent manner, spike bursts, and plateau potentials. The superposition of one large-amplitude EPSP and multiple IPSPs formed one short gamma event in a given thalamic cell.

Sensory-evoked postsynaptic events in VPM cells

Thalamic drivers are a known source of large-amplitude excitatory postsynaptic potentials in VPM cells (Brecht and Sakmann, 2002; Castro-Alamancos, 2002). In adult rats, subthreshold responses (EPSPs and IPSPs) in VPM cells could always be elicited from several adjacent whiskers and lasted for hundreds of milliseconds (Brecht and Sakmann, 2002). In adult anesthetized rodents, the spontaneous postsynaptic activity of many thalamic VPM and LGN cells was represented by a persistent flow of large-amplitude EPSPs (Deschenes et al., 2003; Sheroziya and Timofeev, 2014, 2015). Rhythmic EPSPs of prethalamic origin have been reported in the ventroposterior nuclei of the thalamus (Pinault and Deschenes, 1992; Nunez et al., 1994). Whisker-related neurons in the sensory trigeminal complex of adult rats can generate rhythmic activity; in particular, neurons of the nuclei principalis generated a ~10 Hz rhythm (Panetsos and Sanchez-Jimenez, 2010). Importantly, neurons of the trigeminal complex generated LTS and displayed intrinsic oscillatory properties in slices of adult animals and pups (Sandler et al., 1998; Lo et al., 1999; Lo and Erzurumlu, 2001). It is unclear whether electrically coupled thalamocortical cells (reported coupling coefficient at P6-7 was ~0.02) in rodent pups (Lee et al., 2010) can contribute to EPSPs in VPM cells. Thus, according to our current knowledge, the sensory-evoked EPSPs shown here were generated by synaptic inputs from the trigeminal complex. Sensory-evoked EPSPs produced long-lasting spiking responses in our experiments. In adult animals, only the subthreshold response lasted hundreds of milliseconds, while the spiking response was usually restricted to a short time window (Hartings and Simons, 2000; Brecht and Sakmann, 2002). The absence of postsynaptic GABA(B) receptor-mediated current (Luhmann and Prince, 1991; Nurse and Lacaille, 1999) is a likely reason for long-lasting spiking responses in the immature thalamus.

Whisker-specific segregation is already established in VPM cells by P4-5 in rodents (Belford and Killackey, 1979; Yamakado, 1985; Munoz et al., 1999). Developmental remodeling of the sensory inputs involves synapse formation, then local pruning of subsets of axonal branches and synapse elimination (Chen and Regehr, 2000; Arsenault and Zhang, 2006; Takeuchi et al., 2014). In thalamic slices of adult mice, most of the VPM neurons showed an all-or-none EPSC following medial lemniscus stimulation; while in pups, thalamic neurons displayed an incremental increase in EPCS amplitude with stronger stimulus intensities. Onsets of EPSCs from different axons were indistinguishable, and the number of immature inputs was usually estimated with the number of discrete steps in EPSC amplitude. The number of lemniscal synapses increases during the first postnatal week and decreases after P7-9 (Takeuchi et al., 2014). The mean estimated number of lemniscal axons innervating each VPM neuron was 7–8 at P7-9 and 1–3 in adult rodents (Deschenes et al., 2003; Arsenault and Zhang, 2006; Takeuchi et al., 2014). The maximal amplitude of AMPA-EPSC evoked with medial lemniscus stimulation at −70 mV was ~400 pA at P7-9 and ~1000 pA after P11-13 (Arsenault and Zhang, 2006). On the other hand, the input resistance of thalamic relay cells decreases by 2–3-fold between P6-7 and after P12-14 (Ramoa and McCormick, 1994b; Lee et al., 2010), so the amplitudes of the postsynaptic potentials (at the first approximation proportional to a product of input resistance and postsynaptic current) should not show a dramatic increase with development. In our data, the first sensory-evoked large-amplitude excitatory event was always shunted with inhibition, and succeeding large-amplitude excitatory events had the shape of unit postsynaptic events. In adult rats, trigeminothalamic cell firing depends on amplitude, velocity, and direction of vibrissal deflection (Deschenes et al., 2003). Here, we used a 200-ms-long stimulus and showed prolonged responses in thalamic VPM cells. Firstly, sensory-evoked poststimulus thalamic activities might directly support early cortical activities (Khazipov et al., 2004). Second, the repetition of sensory-evoked signals might be important in the developmental maturation of the thalamocortical network (Minlebaev et al., 2011).

The electrophysiological impact of recently discovered interneurons in different nuclei of the rodent thalamus (Jager et al., 2021) remains unclear; thus, the sensory-evoked IPSPs in our experiments likely originated from TRN (Arcelli et al., 1997; Fogerson and Huguenard, 2016). Compared to the excitatory response, the duration of the inhibitory response in VPM cells was shorter, presumably because the late non-correlated activity of different VPM cells could not activate TRN cells. Due to the shorter duration of the inhibitory response, we could compare the effects of mixed postsynaptic events and pure excitatory events (below).

Interaction of postsynaptic events and the intrinsic membrane currents

In thalamic slices of newborn rats, stimulation of the optic tract evoked EPSPs that gave rise to a plateau potential accompanied by a depolarization block of fast sodium channels. Noninvasive juxtacellular recordings confirmed the partial inactivation of action potentials. Synaptically evoked plateau potential relied on NMDA current and was mediated by L-type calcium channels (Lo et al., 2002; Dilger et al., 2011; Dilger et al., 2015). In our experiments, one large-amplitude EPSP could produce weak LTS without spikes, a spike burst, and short plateau potential. Suprathreshold activities, spike bursts, and plateau potentials could also be mediated with L-type calcium channels and possible electrical contacts between thalamic cells (Lo et al., 2002; Lee et al., 2010; Dilger et al., 2011). Juxtacellular recordings confirmed the partial inactivation of spikes during plateau potential. Intrinsic AHP current (Fig. 5(**D**)) in VPM cells (Pirchio et al., 1997) could contribute to the intervals between spike bursts in thalamic cells and define the maximal frequency/occurrence of spike bursts (low-pass filter). Slow

AHP current was also shown in immature cortical neurons (McCormick and Prince, 1987)(McCormick and Prince, 1987).

We observed gamma-modulated spiking activity, and the whole-cell recordings revealed the contribution of hyperpolarizing events to gamma oscillations. Gamma-modulated IPSPs could either decrease spike frequency/occurrence within bursts or prevent the inactivation of fast sodium channels during plateau potential; as a result, VPM cells could reproduce the rhythm of a presynaptic inhibitory cell. On average, the gamma hot spots marked in the spectrograms corresponded to the first, second, and third large-amplitude EPSP within each sensory response. Firstly, each hot spot could be a result of the direct short-term inhibitory feedback from the TRN. Second, inhibitory postsynaptic currents (and corresponding extracellular potentials) are stronger with the depolarization of postsynaptic cells. The frequency/location of hot spots decreased with its serial number (graded gamma activity). Sensory-evoked EPSPs in different VPM cells tended to form similar inter-EPSP intervals at the beginning of the response. We may propose that the synchrony of independently-generated EPSPs in neighboring VPM cells decreased with the EPSP serial number. The latter can reduce the firing rate in corresponding inhibitory TRN cells and produce a gradual decrease in gamma frequency. On the other hand, the absence of the initial hot spot but the presence of the second and the third indicates high synchrony of the first EPSPs in neighboring VPM cells and subsequent strong inhibitory feedback from the TRN at the beginning of a response. We also observed sensory-evoked graded gamma activity in the barrel cortex at the LFP level (Fig. S5). We propose that the immature thalamus transmitted sensory signals to the cortex through short gamma oscillations patterned by gamma-rhythmic GABAergic input from TRN that is consistent with a suppression of the early cortical gamma oscillations after intrathalamic blockade of GABA(A) receptors (Minlebaev et al., 2011). Immature neurons generate broad action potentials of smaller amplitude compared to mature activity (see Introduction), which points to weak fast sodium and fast potassium currents. Relatively strong excitatory postsynaptic events could induce a depolarization block in our experiments because the fast potassium current was weak. IPSPs prevented the inactivation of spikes and de facto substituted fast potassium current in immature thalamic cells. This mechanism needs investigation *in vitro*.

Latencies of thalamic responses

We detected a relatively large range in latencies of thalamic responses recorded with extracellular electrodes (juxtacellular spikes and MUA). Compared to sensory-evoked responses in adult animals, thalamic responses in neonates (Yang et al., 2013) have significantly longer latencies and, accordingly, have a larger range in the latencies. Technically, the latency detected with a MUA peristimulus time histogram is the latency of the cell with the shortest latency (the left tail of the distribution for cells) and the latency of the fastest responses (the left tail of the distribution for responses). The probability of recording the cell with the shortest latency or the probability of recording only the fastest responses with a juxtacellular electrode is close to zero. It is a possible reason why the latency of spike responses was longer compared to minimal MUA latency (29.9 ± 4.2 ms vs. 23 ± 1 ms, respectively).

On the other hand, channels of a silicon probe with stronger MUA responses displayed shorter (minimal) latencies, while boundary channels with weaker MUA responses displayed longer (maximal) latencies. Firstly, the latencies of MUA responses (in the center of the barreloid and closer to its border) could technically (see above) depend on the local density of responding cells around the electrode. More importantly, lateral inhibition (Pinault and Deschenes, 1998; Lavallee and Deschenes, 2004) might aim home barreloids in the immature thalamus. Lateral inhibition could not be tuned in the immature thalamus, at the least, because IPSPs prevented the inactivation of spikes. We propose that immature lateral inhibition could detain the generation of the first sensory-evoked spike in the cells in boundary areas of the home barreloid. The latter could significantly increase the range in the latencies.

Intrinsic neuronal oscillations and spindle-bursts in the immature thalamus

We used urethane-anesthetized animals in the present study. Urethane might decrease overall network excitability by potentiating the functions of GABA and glycine receptors and by depression of glutamatergic receptors, but it also potentiates the functions of acetylcholine receptors (Hara and Harris, 2002; Pagliardini et al., 2013). Urethane was not a reason for weak intrinsic membrane currents in immature thalamic cells in our experiments because the phenomenon is well documented in slices of newborn animals (see Introduction). With development, voltage-gated sodium channels cluster at the axonal initial segment (Zhou et al., 1998; Jenkins and Bennett, 2001; Garrido et al., 2003; Hedstrom et al., 2007; Kuba et al., 2014; Akter et al., 2020) that is required for mature action potential firing. Intracellular pipettes and the pipette solution itself can change the intrinsic properties of small neurons with high input resistance (Tyzio et al., 2003); therefore, noninvasive juxtacellular recordings are required for the verification of weak intrinsic properties. Among our juxtacellular recordings, only one exhibited spontaneous bursting activity (Fig. S4), and the bursts fulfilled the extracellular criteria of LTS bursts. LTS-related current has short ascending and long descending phases, so spikes occur during the descending phase. Because LTS-related current weakens during the descending phase, the instantaneous spike frequency decreases in a given burst (Lenz et al., 1994; Jeanmonod et al., 1996). In contrast to immature thalamocortical cells, immature TRN cells in slices displayed relatively prominent intrinsic oscillatory properties (intrinsic LTS bursts) at room temperature 20–22 °C (Wang et al., 2010), but intrathalamic TRN-dependent inhibition was weak in rodent pups compared to adult ani-

mals (Evrard and Ropert, 2009; Lee et al., 2010). Here, we detected neither spontaneous nor sensory-evoked sleep spindles in the VPM thalamic nucleus of rat pups, which is in line with weak intrinsic oscillatory properties of thalamocortical cells and weak inhibitory feedback from TRN in the immature thalamus.

Spontaneous and sensory-triggered alpha/beta oscillations (called spindle-bursts) were first detected in the rodent somatosensory cortex (Khazipov et al., 2004) and then in the visual (Hanganu et al., 2006; Colonnese and Khazipov, 2010; Kummer et al., 2016), motor (An et al., 2014) and prefrontal/prelimbic (Brockmann et al., 2011; Bitzenhofer et al., 2015) cortices in postnatal development. With postnatal development, spindle-bursts replace early calcium waves (Martini et al., 2021), and the switch to spindle-bursts correlates with the appearance of active chemical synapses. The generation of spindle-bursts involves the periphery, the thalamus, and the cortex (Khazipov and Milh, 2018). Since higher-order thalamic nuclei form long corticocortical connections, higher-order thalamic nuclei might form the early endogenous pattern generator (Molnar et al., 2020). Spontaneous retinal waves trigger spindle-bursts in the neonatal visual cortex, and removal of the retina reduces the frequency but does not eliminate the cortical spindle-bursts (Hanganu et al., 2006). Subplate neurons and gap junctions are required for spindle-burst oscillations in newborn mice (Dupont et al., 2006). After the selective removal of subplate neurons in the limb region of the primary somatosensory cortex, endogenous and sensory-evoked spindle-bursts were largely abolished (Tolner et al., 2012). The cortex starts generating NMDA-dependent spindle-bursts after the developmental disappearance of the subplate by the end of the first postnatal week (Dupont et al., 2006). In the barrel cortex of urethane anesthetized rats, spontaneous and sensory-evoked spindle-bursts were represented with a negative delta wave nested with fluctuations within the alpha/beta frequency range. Delta wave probably indicated depolarization of cortical cells and was sensitive to glutamatergic AMPA and NMDA receptor antagonists (Minlebaev et al., 2007, 2009).

We observed similar sensory-evoked delta waves with nested oscillations in the barrel cortex. We also detected sensory-evoked waves of smaller magnitude in the thalamus with silicon probes; at the cellular level, the evoked activity was represented mainly by spike bursts and gamma oscillations. Since corticothalamic connections were inactive, we revealed an ascending excitatory component of sensory-evoked thalamic spindle-bursts. The contribution of ascending sensory signals to the generation of cortical spindle-bursts might be similar to the impact of retinal waves on the early oscillations in the visual cortex (Hanganu et al., 2006). Neurons in the whisker-innervating region of the trigeminal ganglion of neonatal mice could generate rare spontaneous activity revealed with calcium imaging (Banerjee et al., 2022). We did not detect spontaneous activity in VPM neurons of anesthetized rat pups, probably because we applied sensory stimuli every 10 s.

Here, we showed an ascending excitatory drive of sensory-evoked thalamic oscillations. Cortical contribution to evoked thalamic activities remained unknown because we removed the cortex in our experiments. A few relatively strong excitatory synapses, weak intrinsic currents, and inhibitory feedback from TRN underlie gamma-modulated activities in immature thalamocortical cells. How thalamic cells generated poststimulus activity is unclear, but we proposed that poststimulus activity depended on intrinsic oscillations in the trigeminal complex.

AUTHOR CONTRIBUTION

MS performed the experiments and analyzed data, MS and RK designed the research project, MS and RK wrote the paper.

DECLARATION OF COMPETING INTEREST

The authors declare that they have no known competing financial interests or personal relationships that could have appeared to influence the work reported in this paper.

ACKNOWLEDGEMENTS

We thank David Jappy for his helpful comments. We thank Dr. Andrei Rozov for the preparation of pipette solutions for patch-clamp recordings and Dr. Andrei Zakharov for technical assistance. We also thank Dr. Igor Timofeev for his critical comments on the manuscript. This work was supported by the Russian Foundation for Basic Research (grant 20–04-00858) for MS.

REFERENCES

Abdul Kadir L, Stacey M, Barrett-Jolley R (2018) Emerging roles of the membrane potential: action beyond the action potential. Front Physiol 9:1661.

Akter N, Fukaya R, Adachi R, Kawabe H, Kuba H (2020) Structural and functional refinement of the axon initial segment in avian cochlear nucleus during development. J Neurosci 40:6709–6721.

An S, Kilb W, Luhmann HJ (2014) Sensory-evoked and spontaneous gamma and spindle bursts in neonatal rat motor cortex. J Neurosci 34:10870–10883.

Arcelli P, Frassoni C, Regondi MC, De Biasi S, Spreafico R (1997) GABAergic neurons in mammalian thalamus: a marker of thalamic complexity? Brain Res Bull 42:27–37.

Arsenault D, Zhang ZW (2006) Developmental remodelling of the lemniscal synapse in the ventral basal thalamus of the mouse. J Physiol-London 573:121–132.

Banerjee P, Kubo F, Nakaoka H, Ajima R, Sato T, Hirata T, Iwasato T (2022) Spontaneous activity in whisker-innervating region of neonatal mouse trigeminal ganglion. Sci Rep 12:16311.

Belford GR, Killackey HP (1979) The development of vibrissae representation in subcortical trigeminal centers of the neonatal rat. J Comp Neurol 188:63–74.

Bitzenhofer SH, Sieben K, Siebert KD, Spehr M, Hanganu-Opatz IL (2015) Oscillatory activity in developing prefrontal networks results from theta-gamma-modulated synaptic inputs. Cell Rep 11:486–497.

Blankenship AG, Feller MB (2010) Mechanisms underlying spontaneous patterned activity in developing neural circuits. Nat Rev Neurosci 11:18–29.
Brecht M, Sakmann B (2002) Whisker maps of neuronal subclasses of the rat ventral posterior medial thalamus, identified by whole-cell voltage recording and morphological reconstruction. J Physiol 538:495–515.
Brockmann MD, Poschel B, Cichon N, Hanganu-Opatz IL (2011) Coupled oscillations mediate directed interactions between prefrontal cortex and hippocampus of the neonatal rat. Neuron 71:332–347.
Buzsaki G, Mizuseki K (2014) The log-dynamic brain: how skewed distributions affect network operations. Nat Rev Neurosci 15:264–278.
Castro-Alamancos MA (2002) Properties of primary sensory (lemniscal) synapses in the ventrobasal thalamus and the relay of high-frequency sensory inputs. J Neurophysiol 87:946–953.
Chen C, Regehr WG (2000) Developmental remodeling of the retinogeniculate synapse. Neuron 28:955–966.
Colonnese MT, Khazipov R (2010) ‘‘Slow activity transients” in infant rat visual cortex: a spreading synchronous oscillation patterned by retinal waves. J Neurosci 30:4325–4337.
Crunelli V, Cope DW, Hughes SW (2006) Thalamic T-type Ca2+ channels and NREM sleep. Cell Calcium 40:175–190.
Deschenes M, Timofeeva E, Lavallee P (2003) The relay of high-frequency sensory signals in the Whisker-to-barreloid pathway. J Neurosci 23:6778–6787.
Dilger EK, Shin HS, Guido W (2011) Requirements for synaptically evoked plateau potentials in relay cells of the dorsal lateral geniculate nucleus of the mouse. J Physiol 589:919–937.
Dilger EK, Krahe TE, Morhardt DR, Seabrook TA, Shin HS, Guido W (2015) Absence of plateau potentials in dLGN cells leads to a breakdown in retinogeniculate refinement. J Neurosci 35:3652–3662.
Dominguez S, Ma L, Yu H, Pouchelon G, Mayer C, Spyropoulos GD, Cea C, Buzsaki G, Fishell G, Khodagholy D, Gelinas JN (2021) A transient postnatal quiescent period precedes emergence of mature cortical dynamics. Elife 10.
Dupont E, Hanganu IL, Kilb W, Hirsch S, Luhmann HJ (2006) Rapid developmental switch in the mechanisms driving early cortical columnar networks. Nature 439:79–83.
Erzurumlu RS, Gaspar P (2012) Development and critical period plasticity of the barrel cortex. Eur J Neurosci 35:1540–1553.
Evrard A, Ropert N (2009) Early development of the thalamic inhibitory feedback loop in the primary somatosensory system of the newborn mice. J Neurosci 29:9930–9940.
Fanselow EE, Sameshima K, Baccala LA, Nicolelis MA (2001) Thalamic bursting in rats during different awake behavioral states. Proc Natl Acad Sci U S A 98:15330–15335.
Fernandez LMJ, Luthi A (2020) Sleep Spindles: Mechanisms and Functions. Physiol Rev 100:805–868.
Fogerson PM, Huguenard JR (2016) Tapping the brakes: cellular and synaptic mechanisms that regulate thalamic oscillations. Neuron 92:687–704.
Ganmor E, Katz Y, Lampl I (2010) Intensity-dependent adaptation of cortical and thalamic neurons is controlled by brainstem circuits of the sensory pathway. Neuron 66:273–286.
Garrido JJ, Giraud P, Carlier E, Fernandes F, Moussif A, Fache MP, Debanne D, Dargent B (2003) A targeting motif involved in sodium channel clustering at the axonal initial segment. Science 300:2091–2094.
Glykys J, Dzhala VI, Kuchibhotla KV, Feng G, Kuner T, Augustine G, Bacskai BJ, Staley KJ (2009) Differences in cortical versus subcortical GABAergic signaling: a candidate mechanism of electroclinical uncoupling of neonatal seizures. Neuron 63:657–672.
Golshani P, Goncalves JT, Khoshkhoo S, Mostany R, Smirnakis S, Portera-Cailliau C (2009) Internally mediated developmental desynchronization of neocortical network activity. J Neurosci 29:10890–10899.
Groh A, Bokor H, Mease RA, Plattner VM, Hangya B, Stroh A, Deschenes M, Acsady L (2014) Convergence of cortical and sensory driver inputs on single thalamocortical cells. Cereb Cortex 24:3167–3179.
Guido W, Weyand T (1995) Burst responses in thalamic relay cells of the awake behaving cat. J Neurophysiol 74:1782–1786.
Hanganu IL, Ben-Ari Y, Khazipov R (2006) Retinal waves trigger spindle bursts in the neonatal rat visual cortex. J Neurosci 26:6728–6736.
Hara K, Harris RA (2002) The anesthetic mechanism of urethane: the effects on neurotransmitter-gated ion channels. Anesth Analg 94:313–318. table of contents.
Hartings JA, Simons DJ (2000) Inhibition suppresses transmission of tonic vibrissa-evoked activity in the rat ventrobasal thalamus. J Neurosci 20:RC100.
Hedstrom KL, Xu X, Ogawa Y, Frischknecht R, Seidenbecher CI, Shrager P, Rasband MN (2007) Neurofascin assembles a specialized extracellular matrix at the axon initial segment. J Cell Biol 178:875–886.
Hirsch JC, Fourment A, Marc ME (1983) Sleep-related variations of membrane potential in the lateral geniculate body relay neurons of the cat. Brain Res 259:308–312.
Huguenard JR, Hamill OP, Prince DA (1988) Developmental changes in Na+ conductances in rat neocortical neurons: appearance of a slowly inactivating component. J Neurophysiol 59:778–795.
Hwang K, Bertolero MA, Liu WB, D’Esposito M (2017) The Human Thalamus Is an Integrative Hub for Functional Brain Networks. J Neurosci 37:5594–5607.
Jager P, Moore G, Calpin P, Durmishi X, Salgarella I, Menage L, Kita Y, Wang Y, Kim DW, Blackshaw S, Schultz SR, Brickley S, Shimogori T, Delogu A (2021) Dual midbrain and forebrain origins of thalamic inhibitory interneurons. Elife 10.
Jahnsen H, Llinas R (1984) Ionic basis for the electro-responsiveness and oscillatory properties of guinea-pig thalamic neurones in vitro. J Physiol 349:227–247.
Jeanmonod D, Magnin M, Morel A (1996) Low-threshold calcium spike bursts in the human thalamus. Common physiopathology for sensory, motor and limbic positive symptoms. Brain 119(Pt 2):363–375.
Jenkins SM, Bennett V (2001) Ankyrin-G coordinates assembly of the spectrin-based membrane skeleton, voltage-gated sodium channels, and L1 CAMs at Purkinje neuron initial segments. J Cell Biol 155:739–746.
Khazipov R, Milh M (2018) Early patterns of activity in the developing cortex: focus on the sensorimotor system. Semin Cell Dev Biol 76:120–129.
Khazipov R, Sirota A, Leinekugel X, Holmes GL, Ben-Ari Y, Buzsaki G (2004) Early motor activity drives spindle bursts in the developing somatosensory cortex. Nature 432:758–761.
Khazipov R, Zaynutdinova D, Ogievetsky E, Valeeva G, Mitrukhina O, Manent JB, Represa A (2015) Atlas of the postnatal rat brain in stereotaxic coordinates. Front Neuroanat 9:161.
Kuba H, Adachi R, Ohmori H (2014) Activity-dependent and activity-independent development of the axon initial segment. J Neurosci 34:3443–3453.
Kummer M, Kirmse K, Zhang C, Haueisen J, Witte OW, Holthoff K (2016) Column-like Ca(2+) clusters in the mouse neonatal neocortex revealed by three-dimensional two-photon Ca(2+) imaging in vivo. Neuroimage 138:64–75.
Lavallee P, Deschenes M (2004) Dendroarchitecture and lateral inhibition in thalamic barreloids. J Neurosci 24:6098–6105.
Lee SC, Cruikshank SJ, Connors BW (2010) Electrical and chemical synapses between relay neurons in developing thalamus. J Physiol 588:2403–2415.
Lenz FA, Kwan HC, Martin R, Tasker R, Richardson RT, Dostrovsky JO (1994) Characteristics of somatotopic organization and spontaneous neuronal activity in the region of the thalamic principal sensory nucleus in patients with spinal cord transection. J Neurophysiol 72:1570–1587.
Llinas RR, Steriade M (2006) Bursting of thalamic neurons and states of vigilance. J Neurophysiol 95:3297–3308.

Lo FS, Erzurumlu RS (2001) Neonatal deafferentation does not alter membrane properties of trigeminal nucleus principalis neurons. J Neurophysiol 85:1088–1096.
Lo FS, Guido W, Erzurumlu RS (1999) Electrophysiological properties and synaptic responses of cells in the trigeminal principal sensory nucleus of postnatal rats. J Neurophysiol 82:2765–2775.
Lo FS, Ziburkus J, Guido W (2002) Synaptic mechanisms regulating the activation of a Ca(2+)-mediated plateau potential in developing relay cells of the LGN. J Neurophysiol 87:1175–1185.
Luhmann HJ, Prince DA (1991) Postnatal maturation of the GABAergic system in rat neocortex. J Neurophysiol 65:247–263.
Luhmann HJ, Khazipov R (2018) Neuronal activity patterns in the developing barrel cortex. Neuroscience 368:256–267.
Luhmann HJ, Reiprich RA, Hanganu I, Kilb W (2000) Cellular physiology of the neonatal rat cerebral cortex: intrinsic membrane properties, sodium and calcium currents. J Neurosci Res 62:574–584.
Marcano-Reik AJ, Blumberg MS (2008) The corpus callosum modulates spindle-burst activity within homotopic regions of somatosensory cortex in newborn rats. Eur J Neurosci 28:1457–1466.
Marlinski V, Beloozerova IN (2014) Burst firing of neurons in the thalamic reticular nucleus during locomotion. J Neurophysiol 112:181–192.
Martini FJ, Guillamon-Vivancos T, Moreno-Juan V, Valdeolmillos M, Lopez-Bendito G (2021) Spontaneous activity in developing thalamic and cortical sensory networks. Neuron 109:2519–2534.
McCormick DA, Prince DA (1987) Post-natal development of electrophysiological properties of rat cerebral cortical pyramidal neurones. J Physiol 393:743–762.
McCormick DA, Trent F, Ramoa AS (1995) Postnatal development of synchronized network oscillations in the ferret dorsal lateral geniculate and perigeniculate nuclei. J Neurosci 15:5739–5752.
Mease RA, Sumser A, Sakmann B, Groh A (2016) Cortical dependence of whisker responses in posterior medial thalamus in vivo. Cereb Cortex 26:3534–3543.
Minlebaev M, Ben-Ari Y, Khazipov R (2007) Network mechanisms of spindle-burst oscillations in the neonatal rat barrel cortex in vivo. J Neurophysiol 97:692–700.
Minlebaev M, Ben-Ari Y, Khazipov R (2009) NMDA receptors pattern early activity in the developing barrel cortex in vivo. Cereb Cortex 19:688–696.
Minlebaev M, Colonnese M, Tsintsadze T, Sirota A, Khazipov R (2011) Early gamma oscillations synchronize developing thalamus and cortex. Science 334:226–229.
Molnar Z, Luhmann HJ, Kanold PO (2020) Transient cortical circuits match spontaneous and sensory-driven activity during development. Science 370.
Munoz A, Liu XB, Jones EG (1999) Development of metabotropic glutamate receptors from trigeminal nuclei to barrel cortex in postnatal mouse. J Comp Neurol 409:549–566.
Murata Y, Colonnese MT (2018) Thalamus controls development and expression of arousal states in visual cortex. J Neurosci 38:8772–8786.
Murata Y, Colonnese MT (2019) Thalamic inhibitory circuits and network activity development. Brain Res 1706:13–23.
Nunez A, Barrenechea C, Avendano C (1994) Spontaneous activity and responses to sensory stimulation in ventrobasal thalamic neurons in the rat: an in vivo intracellular recording and staining study. Somatosens Mot Res 11:89–98.
Nurse S, Lacaille JC (1999) Late maturation of GABA(B) synaptic transmission in area CA1 of the rat hippocampus. Neuropharmacology 38:1733–1742.
Pagliardini S, Gosgnach S, Dickson CT (2013) Spontaneous sleep-like brain state alternations and breathing characteristics in urethane anesthetized mice. PLoS One 8:e70411.
Panetsos F, Sanchez-Jimenez A (2010) Single unit oscillations in rat trigeminal nuclei and their control by the sensorimotor cortex. Neuroscience 169:893–905.
Perez Velazquez JL, Carlen PL (1996) Development of firing patterns and electrical properties in neurons of the rat ventrobasal thalamus. Brain Res Dev Brain Res 91:164–170.
Pinault D, Deschenes M (1992) The origin of rhythmic fast subthreshold depolarizations in thalamic relay cells of rats under urethane anaesthesia. Brain Res 595:295–300.
Pinault D, Deschenes M (1998) Anatomical evidence for a mechanism of lateral inhibition in the rat thalamus. Eur J Neurosci 10:3462–3469.
Pirchio M, Turner JP, Williams SR, Asprodini E, Crunelli V (1997) Postnatal development of membrane properties and delta oscillations in thalamocortical neurons of the cat dorsal lateral geniculate nucleus. J Neurosci 17:5428–5444.
Ramcharan EJ, Gnadt JW, Sherman SM (2000) Burst and tonic firing in thalamic cells of unanesthetized, behaving monkeys. Vis Neurosci 17:55–62.
Ramoa AS, McCormick DA (1994a) Enhanced activation of Nmda receptor responses at the immature retinogeniculate synapse. J Neurosci 14:2098–2105.
Ramoa AS, McCormick DA (1994b) Developmental changes in electrophysiological properties of LGNd neurons during reorganization of retinogeniculate connections. J Neurosci 14:2089–2097.
Sandler VM, Puil E, Schwarz DW (1998) Intrinsic response properties of bursting neurons in the nucleus principalis trigemini of the gerbil. Neuroscience 83:891–904.
Sherman SM (2001) Tonic and burst firing: dual modes of thalamocortical relay. Trends Neurosci 24:122–126.
Sherman SM, Guillery RW (1996) Functional organization of thalamocortical relays. J Neurophysiol 76:1367–1395.
Sherman SM, Guillery RW (1998) On the actions that one nerve cell can have on another: distinguishing ‘‘drivers” from ‘‘modulators”. Proc Natl Acad Sci U S A 95:7121–7126.
Sheroziya M, Timofeev I (2014) Global intracellular slow-wave dynamics of the thalamocortical system. J Neurosci 34:8875–8893.
Sheroziya M, Timofeev I (2015) Moderate cortical cooling eliminates thalamocortical silent states during slow oscillation. J Neurosci 35:13006–13019.
Steriade M, McCormick DA, Sejnowski TJ (1993) Thalamocortical oscillations in the sleeping and aroused brain. Science 262:679–685.
Takeuchi Y, Asano H, Katayama Y, Muragaki Y, Imoto K, Miyata M (2014) Large-scale somatotopic refinement via functional synapse elimination in the sensory thalamus of developing mice. J Neurosci 34:1258–1270.
Tennigkeit F, Schwarz DW, Puil E (1998) Postnatal development of signal generation in auditory thalamic neurons. Brain Res Dev Brain Res 109:255–263.
Timofeev I, Chauvette S (2013) The spindles: are they still thalamic? Sleep 36:825–826.
Tolner EA, Sheikh A, Yukin AY, Kaila K, Kanold PO (2012) Subplate neurons promote spindle bursts and thalamocortical patterning in the neonatal rat somatosensory cortex. J Neurosci 32:692–702.
Tyzio R, Ivanov A, Bernard C, Holmes GL, Ben-Ari Y, Khazipov R (2003) Membrane potential of CA3 hippocampal pyramidal cells during postnatal development. J Neurophysiol 90:2964–2972.
Urbain N, Fourcaud-Trocme N, Laheux S, Salin PA, Gentet LJ (2019) Brain-state-dependent modulation of neuronal firing and membrane potential dynamics in the somatosensory thalamus during natural sleep. Cell Rep 26(1443–1457):e1445.
Urbain N, Salin PA, Libourel PA, Comte JC, Gentet LJ, Petersen CCH (2015) Whisking-related changes in neuronal firing and membrane potential dynamics in the somatosensory thalamus of awake mice. Cell Rep 13:647–656.
Vitali I, Jabaudon D (2014) Synaptic biology of barrel cortex circuit assembly. Semin Cell Dev Biol 35:156–164.
Wang X, Yu G, Hou X, Zhou J, Yang B, Zhang L (2010) Rebound bursts in GABAergic neurons of the thalamic reticular nucleus in postnatal mice. Physiol Res 59:273–280.

Warren RA, Jones EG (1997) Maturation of neuronal form and function in a mouse thalamo-cortical circuit. J Neurosci 17:277–295.

Wei H, Bonjean M, Petry HM, Sejnowski TJ, Bickford ME (2011) Thalamic burst firing propensity: a comparison of the dorsal lateral geniculate and pulvinar nuclei in the tree shrew. J Neurosci 31:17287–17299.

Yakovlev AV, Koroleva KS, Valiullina FF, Khazipov RN (2013) Resting membrane potential of rat ventroposteriomedial thalamic neurons during postnatal development. Biochem (Moscow) Suppl Ser A: Membr Cell Biol 7:207–212.

Yamakado M (1985) Postnatal development of barreloid neuropils in the ventrobasal complex of mouse thalamus: a histochemical study for cytochrome oxidase. No To Shinkei 37:497–506.

Yang J-W, Hanganu-Opatz IL, Sun J-J, Luhmann HJ (2009) Three patterns of oscillatory activity differentially synchronize developing neocortical networks in vivo. J Neurosci 29:9011–9025.

Yang JW, An S, Sun JJ, Reyes-Puerta V, Kindler J, Berger T, Kilb W, Luhmann HJ (2013) Thalamic network oscillations synchronize ontogenetic columns in the newborn rat barrel cortex. Cereb Cortex 23:1299–1316.

Zhou D, Lambert S, Malen PL, Carpenter S, Boland LM, Bennett V (1998) AnkyrinG is required for clustering of voltage-gated Na channels at axon initial segments and for normal action potential firing. J Cell Biol 143:1295–1304.

APPENDIX A. SUPPLEMENTARY DATA

Supplementary data to this article can be found online at https://doi.org/10.1016/j.neuroscience.2023.09.005.

(Received 10 June 2023, Accepted 8 September 2023)
(Available online 26 September 2023)